arXiv:1408.2532v2 [nucl-ex] 21 Aug 2014

Collective Expansion at the LHC: selected ALICE anisotropic flow measurements

Raimond Snellings[1,2]

[1] Utrecht University, Princetonplein 5, 3508 TA Utrecht, The Netherlands.
[2] Nikhef, Sciencepark 105, 1098 XG Amsterdam, The Netherlands.

E-mail: Raimond.Snellings@cern.ch

Abstract.

The collective expansion of matter created in collisions of heavy-ions, ranging from collision energies of tens of MeV to a few TeV per nucleon pair, proved to be one of the best probes to study the detailed properties of these unknown states of matter. Collective expansion originates from the initial pressure gradients in the created hot and dense matter. These pressure gradients transform the initial spatial deformations and inhomogeneities of the created matter into momentum anisotropies of the final state particle production, which we call anisotropic flow. These momentum anisotropies are experimentally characterised by so-called flow harmonics. In this paper I review ALICE measurements of the flow harmonics at the CERN Large Hadron Collider and discuss some of the open questions.

1. INTRODUCTION

In the world around us, quarks and gluons do not exist as free particles because they are permanently bound into hadrons by the strong interaction. At very high temperatures and densities however, hadronic matter is expected to undergo a phase transition to a new state of matter, the Quark-Gluon Plasma (QGP), where quark and gluon degrees of freedom are not anymore confined inside the hadrons [1, 2, 3, 4, 5, 6, 7, 8]. Such temperatures and densities were present in the early Universe until the first microseconds after the Big Bang. Not only in the early Universe, but also in heavy-ion collisions at ultra-relativistic energies it is possible to reach temperatures and energy densities well above the phase-transition point. The highest temperatures and energy densities are currently reached in collisions of heavy-ions at the Large Hadron Collider (LHC).

Measurements of the collective expansion of the QGP, in particular the azimuthal anisotropies in the expansion [9], provide us with constraints on the properties of the system such as the equation of state (EoS) [10] and transport coefficients like the kinematic viscosity, defined as the shear viscosity over entropy ratio (η/s). The collective expansion, also called flow, originates from the initial pressure gradients in the created hot and dense matter. These pressure gradients transform the initial spatial deformations and inhomogeneities of the created matter into momentum anisotropies of the final state particle production, which are experimentally characterised by so-called flow harmonics [11]. For recent reviews see [12, 13, 14, 15, 16, 17]

Based on asymptotic freedom [18, 19] in Quantum Chromo Dynamics (QCD) and color Debye screening [20], the properties of the QGP were expected to be similar to a weakly interacting gas of quarks and gluons. In that case the mean free path in the QGP is large, which implies a large viscosity. A direct consequence of a large viscosity is that the system will not develop strong collective expansion. Therefore the discovery of a very large 2^{nd} order flow harmonic [21, 22], called elliptic flow, at the Relativistic Heavy Ion Collider (RHIC) and more recently at the LHC [23, 24, 25] changed dramatically our understanding of the QGP.

Currently, the buildup of this large flow is theoretically best understood in a relativistic viscous hydrodynamic model description. In these models the large flow is understood by assuming that the system is, very quickly after the collision, in local equilibrium and forms a strongly coupled quark-gluon liquid. Only after it was realised that already a small kinematic viscosity significantly reduces the buildup of the elliptic flow [26, 27, 28], it became clear that the system produced behaves as an almost ideal or inviscid fluid, which is a fluid that has almost no resistance to shear stress.

While lattice QCD calculations can calculate precisely quantities like the EoS of the QGP, they unfortunately currently provide little guidance to dynamical quantities like the kinematic viscosity. It turns out that in a strongly coupled N = 4 super-symmetric Yang Mills theory with a large number of colors (the so-called 't Hooft limit), η/s can be calculated using a gauge gravity duality and is found to be $1/4\pi$ (in natural units). Using the famous AdS/CFT correspondence [29], Kovtun, Son and Starinets conjectured that this value of η/s is a lower bound for all fluids (the KSS bound) [30]. We therefore call a fluid with η/s = $1/4\pi$ a perfect fluid.

For many other fluids, like helium, nitrogen, and water, the transition from one phase to another occurs in the vicinity where the kinematic viscosity has a minimum. Therefore an accurate measurement of the kinematic viscosity as function of the

QGP temperature would help pinpoint the location of the cross over QCD phase transition [31, 32].

After the first observation of the large elliptic flow at RHIC [21] it was quickly realised that reported measurements of the elliptic flow included contributions from event-by-event fluctuations [33], which were not included in the theoretical description. Currently we have strong evidence that these event-by-event fluctuations of the anisotropic flow coefficients are mainly due to the event-by-event fluctuations of the initial spatial deformations and inhomogeneities of the produced matter [33, 34, 35, 36, 37]. The low kinematic viscosity of the QGP makes it possible that traces of these initial spatial distributions survive the complete dynamics of the expansion until the final freeze-out stage. Therefore, measurements of the event-by-event distribution of the flow coefficients (or the mean values and moments of the distribution) and their correlation provide, not only, a unique way to determine the kinematic viscosity of the QGP but also strongly constrain the unknown initial conditions.

The experimental determination of the kinematic viscosity and constraints on the initial conditions can only be achieved with precision flow measurements combined with an accurate model description of the complete dynamics of the produced system, that is from the initial conditions up to the point where the produced particles do not re-interact anymore.

2. HEAVY-ION COLLISIONS

Collisions of heavy ions at LHC energies produce a system with temperatures that are well above the strong phase transition temperature and are therefore a unique tool to create and study hot and dense QCD matter and its phase transition to ordinary hadronic matter in the laboratory. Like the early universe, the hot and dense system created in a heavy-ion collision will expand and cool down. In this time evolution the system probes a range of energy densities and temperatures, and possibly different phases. The evolution of the created system can be divided in two characteristic periods. During the formation of the system collisions with large momentum transfer occur and during this period the largest energy density is created. The system will thermalize and form the QGP provided that the quarks and gluons undergo multiple interactions. Due to the thermal pressure, the system undergoes a collective expansion and eventually becomes so dilute that it hadronizes. In the hadronic phase it further cools down via inelastic and elastic interactions until it becomes non-interacting (the freeze- out stage). This collective expansion we call flow. Therefore, the observation of collective flow signals the presence of multiple interactions between the constituents of the medium produced in the collision. More interactions usually leads to a larger magnitude of the flow and brings the system closer to thermalization. Flow is therefore an observable that provides experimental information on the equation of state and the transport properties of the produced QGP.

Heavy ions are extended objects and the system created in a head-on collision is different from that in a peripheral collision. Therefore, collisions are categorized by their centrality. Theoretically the centrality is characterized by the impact parameter $\mathbf{b}$ (see Fig. 1) which is, however, not a direct observable. Experimentally, the collision centrality can be inferred from the measured particle multiplicities if one assumes that this multiplicity is a monotonic function of $\mathbf{b}$.

In the most central collisions (small impact parameter $\mathbf{b}$) the spatial distribution of the created system is approximately azimuthally symmetric, and the resulting

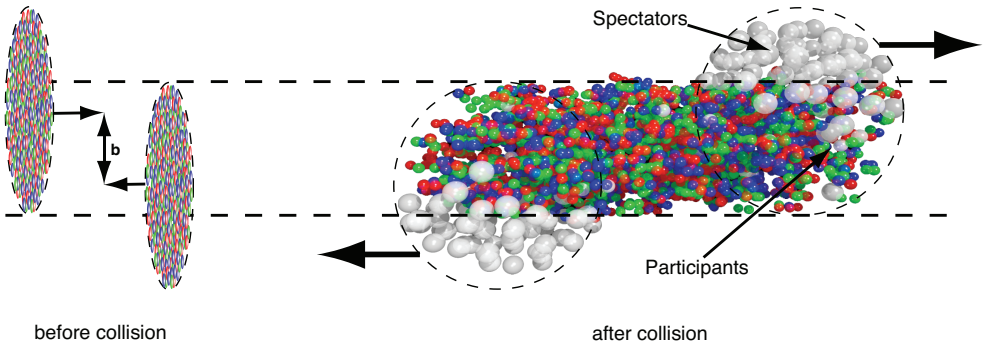

Figure 1. Left: The two heavy-ions before collision with impact parameter **b**. Right: The spectators continue unaffected, while in the participant zone particle production takes place.

azimuthally symmetric expansion is called radial flow. For more peripheral collisions the interaction volume changes roughly into an almond shape and due to its spatial anisotropy the expansion will be different as function of azimuth. This gives rise to so-called anisotropic flow.

3. ANISOTROPIC FLOW

Experimentally, the most direct evidence of collective flow comes from the observation of anisotropic flow, which is the anisotropy in particle momentum distributions correlated with the flow symmetry plane. The various patterns of anisotropic flow are characterised using a Fourier expansion of the event averaged azimuthal particle distribution:

$$\frac{dN}{d\varphi} = \frac{\bar{N}}{2\pi}\left(1 + 2\sum_{n=1}^{\infty} \bar{v}_n \cos(n(\varphi - \bar{\Psi}_n))\right), \tag{1}$$

where $\bar{N} \equiv \langle N \rangle$ is the mean number of selected particles per event, φ the azimuthal angle, and $\bar{\Psi}_n$ the mean angle of the n-th harmonic flow plane.

The Fourier coefficients are in general p_{T} and rapidity (y) dependent and are given by:

$$\begin{aligned} \bar{v}_n(p_{\mathrm{T}}, y) &= \langle\langle \cos[n(\varphi - \bar{\Psi}_n)]\rangle\rangle \quad \text{or equivalently} \\ \bar{v}_n(p_{\mathrm{T}}, y) &= \langle\langle e^{in\varphi} e^{-in\bar{\Psi}_n}\rangle\rangle, \end{aligned} \tag{2}$$

where $\langle\langle \ldots \rangle\rangle$ denotes an average in the (p_{T}, y) bin under study over particles within the same event, and is used in the context of single-particle, two-particle and multi-particle averages, followed by averaging over all events. Since the Fourier series in Eq. 2 is expressed only in terms of cosines, the imaginary part of the second line is zero. In this Fourier decomposition, the coefficients $\bar{v}_1$ and $\bar{v}_2$ are known as directed and elliptic flow, respectively.

3.1. Experimental Methods

Because the flow angle is not a direct observable the anisotropic flow (Eq. 2) can not be measured directly, therefore it is usually estimated using azimuthal correlations

between the observed particles. Two-particle azimuthal correlations, for example, can be written as:

$$\begin{aligned}\langle\langle e^{in(\varphi_1-\varphi_2)}\rangle\rangle &= \langle\langle e^{in(\varphi_1-\bar{\Psi}_n-(\varphi_2-\bar{\Psi}_n))}\rangle\rangle,\\ &= \langle\langle e^{in(\varphi_1-\bar{\Psi}_n)}\rangle\langle e^{-in(\varphi_2-\bar{\Psi}_n)}\rangle + \delta_{2,n}\rangle,\\ &= \langle v_n^2 + \delta_{2,n}\rangle, \end{aligned} \tag{3}$$

In Eq. 3 we have factorized the azimuthal correlation between the particles in a common correlation with the flow angle (anisotropic flow v_n) and a correlation independent of the flow angle (nonflow $\delta_{2,n}$). If $\delta_{2,n}$ is small, Eq. 3 can be used to measure $\langle v_n^2\rangle$, but in general the nonflow contribution is not negligible. These additional nonflow correlations arise from e.g. resonance decays, jet fragmentation, and Bose-Einstein correlations. They can be suppressed by appropriate kinematic cuts (which complicate comparisons between experiments) or by making use of the collective nature of anisotropic flow using multi-particle correlations.

For the latter, this is done using so called cumulants [38], which are genuine multi-particle correlations. For instance, the two-particle cumulant $c_n\{2\}$ and the four-particle cumulants $c_n\{4\}$ are defined as:

$$c_n\{2\} \equiv \left\langle\left\langle e^{in(\varphi_1-\varphi_2)}\right\rangle\right\rangle = \left\langle v_n^2 + \delta_{2,n}\right\rangle, \tag{4}$$

$$\begin{aligned} c_n\{4\} &\equiv \left\langle\left\langle e^{in(\varphi_1+\varphi_2-\varphi_3-\varphi_4)}\right\rangle\right\rangle - 2\left\langle\left\langle e^{in(\varphi_1-\varphi_2)}\right\rangle\right\rangle^2,\\ &= \left\langle v_n^4 + \delta_{4,n} + 4v_n^2\delta_{2,n} + 2\delta_{2,n}^2\right\rangle - 2\left\langle v_n^2 + \delta_{2,n}\right\rangle^2,\\ &= \left\langle -v_n^4 + \delta_{4,n}\right\rangle. \end{aligned} \tag{5}$$

From the combinatorics it is easy to show that $\delta_{2,n} \propto 1/M_\mathrm{c}$ and $\delta_{4,n} \propto 1/M_\mathrm{c}^3$, where M_c is the number of independent particle clusters. Therefore, $v_n\{2\}$ is only a good estimate if $v_n \gg 1/\sqrt{M_\mathrm{c}}$ while $v_n\{4\}$ is already a good estimate of v_n if $v_n \gg 1/{M_\mathrm{c}}^{3/4}$; for $c_n\{\infty\}$ this argument leads to $v_n \gg 1/M_\mathrm{c}$. This shows that for a typical Pb–Pb collision at the LHC with $M_\mathrm{c} = 500$ the possible nonflow contribution can be reduced by more than an order of magnitude using higher order cumulants.

One of the problems in using multi-particle correlations is the computing power needed to go over all possible particle multiplets. To avoid this problem, multi-particle azimuthal correlations in heavy-ion collision are often calculated using so-called Q-cumulants [39, 40]. The Q-cumulants are calculated analytically from a flow vector Q_n:

$$Q_n \equiv \sum_{i=1}^{M} e^{in\varphi_i}, \tag{6}$$

where M is the number of selected particles in an event. In general this flow vector can be constructed using weights for the individual particles and the angle of this flow vector Q_n can be used to estimate the flow angle, similar to the first introduction of Q_n in [41]. As an example we show how the flow vector is used to calculate the two-particle cumulant.

Realising that

$$|Q_n|^2 = \sum_{i,j=1}^{M} e^{in(\varphi_i-\varphi_j)} = M + \sum_{i\neq j} e^{in(\varphi_i-\varphi_j)}, \tag{7}$$

and using this in our definition of the individual event averaged two-particle azimuthal correlation

$$\left\langle e^{in(\varphi_1-\varphi_2)}\right\rangle \equiv \frac{1}{M(M-1)}\sum_{i\neq j} e^{in(\varphi_i-\varphi_j)} = \frac{|Q_n|^2 - M}{M(M-1)}, \tag{8}$$

we immediately see that we can express the individual event average two-particle azimuthal correlation in terms of powers of the flow vector. With the two-particle cumulant defined as the average over all events of Eq 8 we get:

$$\begin{aligned} c_n\{2\} \equiv \left\langle\left\langle e^{in(\varphi_1-\varphi_2)}\right\rangle\right\rangle &\equiv \frac{\sum_{i=1}^{N} M_i(M_i-1)\left\langle e^{in(\varphi_1-\varphi_2)}\right\rangle_i}{\sum_{i=1}^{N} M_i(M_i-1)} \\ &= \frac{\sum_{i=1}^{N} |Q_{in}|^2 - M_i}{\sum_{i=1}^{N} M_i(M_i-1)}, \end{aligned} \tag{9}$$

where N is the number of events. This expression already simplifies the calculation of the two-particle cumulant because it does not require a nested loop over all the particles pairs. For four-particle and higher order cumulants the equations can be found in [39, 40] and for these calculations the gain from using powers of the Q-vector are even bigger.

To relate the two- and multi-particle observables to the flow Fourier coefficients in Eq. 2 we already mentioned that we assumed that the correlation between v_n and $\delta_{2,n}$ is negligible. In addition the assumption was made that $\langle\delta_{2,n}^2\rangle = \langle\delta_{2,n}\rangle^2$ and $\langle v_n^4\rangle = \langle v_n^2\rangle^2$. In other words, we have neglected the event-by-event fluctuations in v_n and $\delta_{2,n}$. The effect of the fluctuations on v_n estimates can be obtained from

$$\begin{aligned} \langle v_n^2\rangle &= \bar{v}_n^2 + \sigma_{v_n}^2, \\ \langle v_n^4\rangle &= \bar{v}_n^4 + 6\sigma_{v_n}^2\bar{v}_n^2, \\ \langle v_n^6\rangle &= \bar{v}_n^6 + 15\sigma_{v_n}^2\bar{v}_n^4, \end{aligned} \tag{10}$$

where σ_{v_n} is the variance of v_n. Neglecting the nonflow terms we have the following expressions for the cumulants:

$$\begin{aligned} v_n\{2\} &= \sqrt{\langle v_n^2\rangle}, \\ v_n\{4\} &= \sqrt[4]{2\langle v_n^2\rangle^2 - \langle v_n^4\rangle}, \\ v_n\{6\} &= \sqrt[6]{\frac{1}{4}\left(\langle v_n^6\rangle - 9\langle v_n^2\rangle\langle v_n^4\rangle + 12\langle v_n^2\rangle^3\right)}. \end{aligned} \tag{11}$$

Here we have introduced the notation $v_n\{k\}$ as the flow estimate from the cumulant $c_n\{k\}$. In case that $\sigma_{v_n} \ll \bar{v}_n$ we obtain from Eqs. 10 and 11, up to order $\sigma_{v_n}^2$:

$$\begin{aligned} v_n\{2\} &= \bar{v}_n + \frac{1}{2}\frac{\sigma_{v_n}^2}{\bar{v}_n}, \\ v_n\{4\} &= \bar{v}_n - \frac{1}{2}\frac{\sigma_{v_n}^2}{\bar{v}_n}, \\ v_n\{6\} &= \bar{v}_n - \frac{1}{2}\frac{\sigma_{v_n}^2}{\bar{v}_n}. \end{aligned} \tag{12}$$

Equations 5 and 12 illustrate that the difference between $v_n\{2\}$ and $v_n\{4\}$ is sensitive to not only nonflow but also to the event-by-event v_n fluctuations.

3.2. Initial Conditions

The development of anisotropic flow is controlled by the anisotropies in the pressure gradients which in turn depend on the shape and structure of the initial density profile. The latter can be characterised, in analogy with the flow Fourier coefficients and flow angles of Eq. 2, by a set of harmonic eccentricity coefficients ε_n and associated angles Φ_n:

$$\begin{aligned} \varepsilon_1 e^{i\Phi_1} &\equiv -\frac{\int r\,dr\,d\phi\, r^3 e^{i\phi}\, e(r,\phi)}{\int r\,dr\,d\phi\, r^3 e(r,\phi)}, \\ \varepsilon_n e^{in\Phi_n} &\equiv -\frac{\int r\,dr\,d\phi\, r^n e^{in\phi}\, e(r,\phi)}{\int r\,dr\,d\phi\, r^n e(r,\phi)} \;\; (n>1), \end{aligned} \tag{13}$$

where $e(r,\phi)$ is the initial energy density distribution in the plane transverse to the beam direction. It should be noted, however, that these eccentricity coefficients involve only the lowest moments of the initial density profile, describing the large scale structures relevant for the hydrodynamic response.

Even at a fixed impact parameter, due to event-by-event fluctuations of the transverse positions of the nucleons inside the colliding nuclei [33], and of the gluon density profiles inside those nucleons [42, 43, 44, 45, 46, 47, 48] the ε_n and Φ_n vary event-by-event. The event-by-event ε_n and Φ_n control in a hydrodynamic picture the event-by-event anisotropic flow coefficients v_n and their directions Ψ_n. The different cumulants are sensitive to the statistical distribution of these flow coefficients and angles, and can be used to constrain the current uncertainty on the initial conditions.

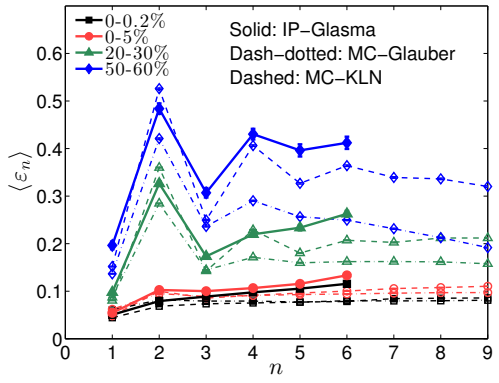

Figure 2. The ε_n rms from three different initial-state models (IP-Glasma, MC-Glauber, MC-KLN) for 2.76 A TeV Pb+Pb collisions of different centralities (figure from [15]).

This is important because in heavy-ion collisions the physics of the initial stage is one of the biggest open questions, and is responsible for the largest uncertainty in many observables. Currently different theoretical models are used to model the initial energy and entropy density. Figure 2 shows the corresponding $\langle\varepsilon_n\rangle$ distribution for the Monte Carlo (MC) Glauber [49], Monte Carlo Kharzeev-Levin-Nardi (MC-KLN) [50]

and IP-Glasma models [51, 52, 42, 43, 53, 44, 45], for four centrality classes. The MC-Glauber is the most common model used.

In the MC-Glauber model the entropy is proportional to the number of interacting nucleons in the two colliding nuclei. The fluctuating event-by-event distribution of these nucleons are in the MC-Glauber model responsible for the fluctuations in ε_n. In the MC-KLN model the entropy is calculated by the initial gluon production, which is position dependent and is calculated based on Color Glass Condensate ideas. Both these models do not take into account fluctuations of the gluon fields inside the colliding nucleons. The IP-Glasma model does take this into account and in addition evolves these gluon fields, using classical Yang-Mills dynamics, to a matching surface after which hydrodynamic model calculations can take over.

In Fig. 2 the $\langle\varepsilon_n\rangle$ are plotted for these three models in different centrality bins. In the most central collisions, 0–0.2%, the ε_n are entirely due to fluctuations, and all $\langle\varepsilon_n\rangle$ have roughly equal magnitudes. For increasingly less central collisions the spatial distribution of the produced system becomes more almond like which is clearly seen by the increase of $\langle\varepsilon_2\rangle$ and also, although to a lesser extend, in $\langle\varepsilon_4\rangle$ and $\langle\varepsilon_6\rangle$. The odd eccentricity coefficients are on the other hand for all centralities dominated by fluctuations.

There is a clear difference between the three models for the full $\langle\varepsilon_n\rangle$ spectrum and measurements of the anisotropic flow coefficients allow us, in principle, to discriminate between these various models of the initial state. This is because the $\langle v_n\rangle$ depend on the anisotropies in the pressure gradients which in turn depend on $\langle\varepsilon_n\rangle$. In addition, the theoretical models also differ in their predictions for the correlations between the eccentricity coefficients $\langle\varepsilon_n\rangle$ (not shown here) which again can be tested experimentally with the correlations between the different $\langle v_n\rangle$. These correlations between eccentricity coefficients $\langle\varepsilon_n\rangle$ are modified through a non-linear viscous hydrodynamics evolution [54, 55, 56], which provides even more interesting tests of the hydrodynamical paradigm.

3.3. Viscous effects on anisotropic flow

Lattice QCD calculations of the equation of state of a QGP showed only small deviations from the Stefan-Boltzmann limit which matched the expectation that the QGP would behave like an massless ideal gas. However, unexpectedly, the experimental data on elliptic flow from RHIC showed good agreement with model predictions from ideal hydrodynamics. This dramatically changed our understanding of the QGP, which resembles, instead of a dilute gas of quarks and gluons, a rather strongly coupled liquid.

While ideal hydrodynamics was very successful, it was only applicable for relatively low transverse momenta and more central collisions. The realisation that small viscous corrections significantly affect the buildup of anisotropic flow [26, 27, 28] triggered the theoretical development of viscous hydrodynamical models [27, 28, 57, 58, 59, 60, 61, 62, 63, 64, 65]. It also triggered the comparison with models of strongly interacting systems such as the AdS/CFT correspondence [29]. These calculations showed that the kinematic viscosity η/s should be very small [30] to explain the observed large elliptic flow and that the EoS of the QGP indeed changes very little from an ideal gas to a strongly coupled system [66].

The shear viscosity reduces the difference between the expansion velocities in the system and therefore reduces the anisotropic flow. This reduction is stronger for larger

n and, as a consequence, the spectrum of v_n coefficients is a very sensitive observable to determine the magnitude of η/s. It is thought that viscous corrections increase for particles with larger transverse momenta. Therefore the measurements of v_n at high transverse momenta are in principle a sensitive probe of η/s. In ideal hydrodynamics switching from a fluid description to a distribution of particles $f(x,p)$ is understood using the Cooper-Frye prescription. For a system which is slightly out of equilibrium, i.e. a viscous system, this process is not so well understood and is modelled with a small deviation from the equilibrium distribution adding a term δf. Because δf increases roughly as ${p_{\rm T}}^{\alpha}$ also the theoretical uncertainties increase with increasing $p_{\rm T}$, therefore the comparison between the v_n coefficients and hydrodynamics are most reliable at small transverse momenta, typically $p_{\rm T} \leq 2$ GeV/c.

4. ANISOTROPIC FLOW MEASUREMENTS FROM ALICE

While the large elliptic flow observed at RHIC provided compelling evidence for strongly interacting matter, a precise determination of η/s in the QGP was complicated by uncertainties in the initial conditions of the collision, the relative contributions to the anisotropic flow from the hadronic and partonic phase, and the unknown temperature dependence of η/s. Because of all these uncertainties it was not even clear if the elliptic flow would increase or decrease when going from RHIC to LHC energies; the first measurement of elliptic flow at the LHC was therefore one of the most anticipated results.

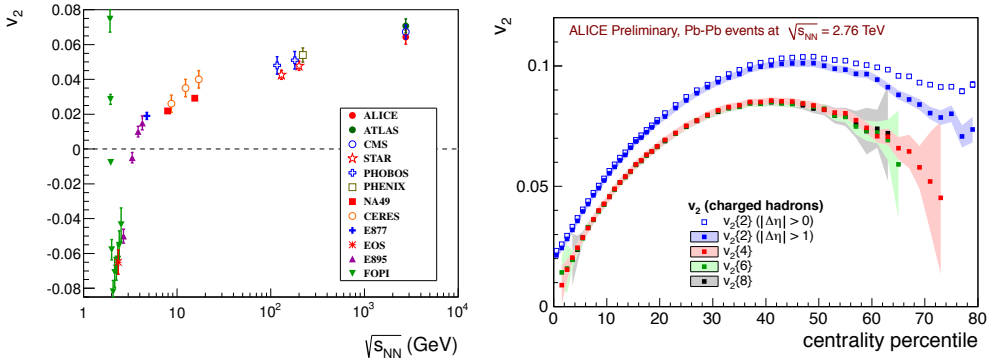

Figure 3. Integrated elliptic flow as a function of collision energy for the 20–30% centrality class (left) [23, 24, 25] and (right) integrated elliptic flow estimates as a function of collision centrality (right figure from [67]).

In the left panel of Fig. 3 the LHC measurements at 2.76 TeV [23, 24, 25] show that the integrated elliptic flow of charged particles increases by about 30% compared to the elliptic flow measured at the highest RHIC energy of 0.2 TeV. This result indicates that the hot and dense matter created in these collisions at the LHC still behaves like a fluid with almost zero friction, and in addition, provides strong constraints on the temperature dependence of η/s.

The centrality dependence, in narrow bins (1–2%) to reduce trivial event-by-event fluctuations, of the elliptic flow at the LHC is plotted in the right panel of Fig. 3. The elliptic flow shows an expected increase with decreasing centrality because of the increasing initial spatial anisotropy of the collision zone. For more peripheral

collisions the elliptic flow starts to decrease again, which is attributed mainly due to larger viscous corrections in the smaller system with larger gradients.

There is a significant difference between flow estimates from two- and multi-particle correlations. This difference is caused by nonflow contributions and by event-by-event fluctuations in the elliptic flow. The effect of the nonflow on two-particle estimates is apparent in more peripheral collisions from the difference in v_2 calculated from the correlation between particles with a gap in pseudorapidity $|\Delta\eta| > 0$ and $|\Delta\eta| > 1$. The results from four-, six-, and eight-particle cumulant estimates which are consistent within uncertainties, indicate that the genuine four-particle, and higher order, nonflow contribution is negligible. The contribution of the event-by-event fluctuations is discussed in the next section.

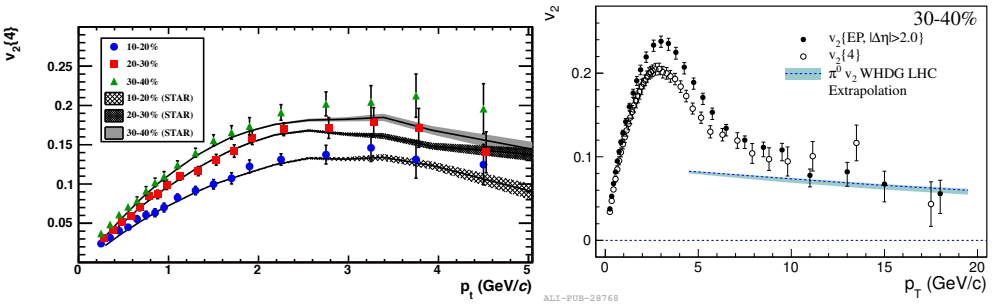

Figure 4. Left: A comparison between p_{T}-differential elliptic flow of charged particles as a function of centrality at RHIC and LHC energies (figure from [23]). Right: p_{T}-differential elliptic flow of charged particles compared to jet energy loss model calculations (figure from [68]).

Elliptic flow as a function of transverse momentum is, compared to integrated flow, more sensitive to the evolution and freeze-out conditions of the produced system. The left panel of Fig. 4 shows the charged particle p_{T}-differential $v_2\{4\}$ measured in ALICE compared to STAR measurements at RHIC. Remarkably, the $v_2(p_{\mathrm{T}})$ is the same within uncertainties at low p_{T} [23], while the beam energies are different by more than one order of magnitude.

The p_{T}-differential v_2, plotted in the right panel of Fig. 4, is still large above 15 GeV/c. At these relatively high transverse momenta the hadron yields are not from a boosted thermal system but are thought to contain a dominant contribution from the fragmentation of high energy partons produced at initial hard scatterings. These high energy partons traversing the nuclear matter are expected to lose energy, which depends strongly on the color charge density of the matter and on the path length traversed by the partons. Because the spatial shape of the created system is anisotropic this path length depends on the azimuthal emission angle, which introduces an azimuthal anisotropy in the particle emission at large p_{T} [69]. The magnitude of the observed v_2 at high-p_{T} is roughly consistent with model calculations of the effect of parton energy loss for neutral pion production [70].

The 30% increase in the integrated flow, which was shown in the left panel of Fig. 3, is clearly not due to the change of $v_2(p_{\mathrm{T}})$ as function of beam energy and must therefore be due to an increase in average transverse momentum [71]. This increase in $\langle p_{\mathrm{T}} \rangle$ is in a hydrodynamical picture naturally explained by an increase in the radial flow. This modifies the spectra with a blueshift which depends on the mass of the

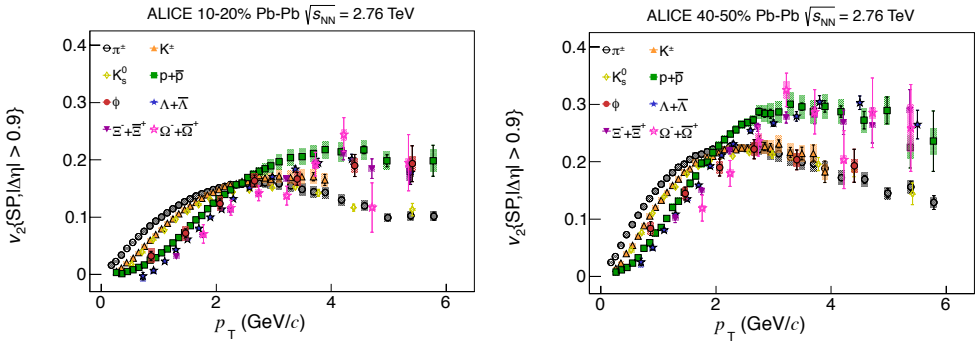
ALICE 10-20% Pb-Pb $\sqrt{s_{NN}}$ = 2.76 TeV
ALICE 40-50% Pb-Pb $\sqrt{s_{NN}}$ = 2.76 TeV
$v_2\{SP,|\Delta\eta|>0.9\}$
p_T (GeV/c)
$\pi^{\pm}$ $K^{\pm}$ K^0_s p+$\bar{p}$ ϕ $\Lambda+\bar{\Lambda}$ $\Xi^-+\bar{\Xi}^+$ $\Omega^-+\bar{\Omega}^+$

Figure 5. p_{T}-differential elliptic flow of identified particles for the 10–20% (left) and 40–50% (right) centrality class (figures from [72]).

particle and leads to flatter p_{T} distributions, particular at low-p_{T}. In hydrodynamics this blueshift is stronger in the direction of the flow plane which results in a depletion of low-p_{T} particles in the direction of this plane. This depletion becomes stronger for increasing particle mass and radial flow, which is the reason that at a fixed value of p_{T} heavier particles have a smaller v_2 (this is also true for other v_n coefficients) compared to lighter ones [73]. Figure 5 shows the v_2 for particles of different mass (with masses which differ by an order of magnitude) for two centralities. A mass ordering is observed, as was also seen in STAR [74], in both centrality bins, left panel 10-20% and right 40-50%, and for all particles. This mass ordering is broken at intermediate p_{T} (2-3 GeV/c) which is not expected in ideal hydrodynamics.

The ϕ-meson is among the particle species of special interest as its mass is very close to the proton and Λ baryons. Below $p_{\mathrm{T}} = 2.5$ GeV/c the ϕ-meson follows within the relatively large uncertainties the mass hierarchy for all centralities. However, for the lowest p_{T} bin there is an indication that the ϕ-meson v_2 is larger than the proton v_2. It is argued that the ϕ-meson has a smaller hadronic interaction cross section,

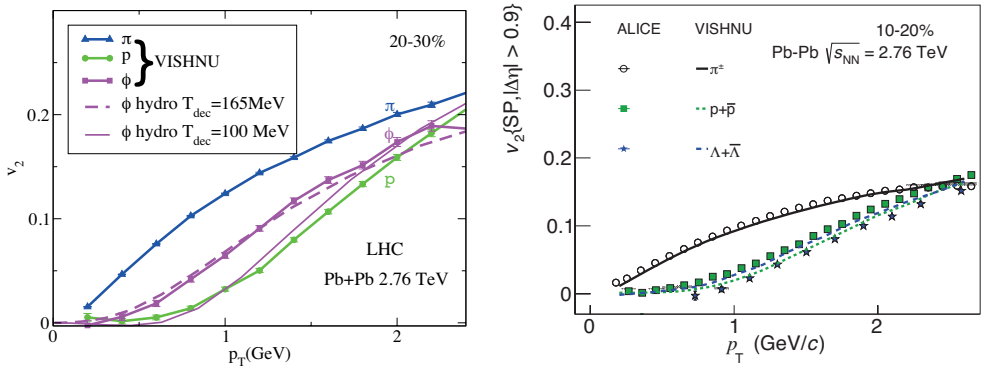

Figure 6. Left: A comparison between VISHNU hybrid model calculations, that couple viscous hydrodynamical calculations to a hadronic transport model, for π, p and ϕ v_2 and a full hydro calculations for the ϕ v_2 with two decoupling temperatures T_{dec} (figure from [75]). Right: A comparison between ALICE measurements and VISHNU hybrid model calculations for the elliptic flow of π, p + $\bar{\mathrm{p}}$ and $\Lambda + \bar{\Lambda}$ (figure from [72]).

which would make it less affected by the late hadronic stage of the collision. It would therefore build up less radial flow than the other particles and this would break the mass hierarchy of v_2. In the left panel of Fig. 6 the VISHNU [75] predictions for v_2 as function of transverse momentum are plotted for pions, protons and the ϕ-meson. VISHNU is a hybrid model calculation which matches a $(2+1)$-dimensional longitudinally boost-invariant viscous hydrodynamic calculation to a hadron cascade model (UrQMD). In this hybrid model the Cooper-Frye algorithm is used to convert the hydrodynamical system into particle phase-space distributions on a switching surface of constant temperature $T_{\rm chem}$, assuming chemical equilibrium particle yields. The hadron cascade UrQMD then propagates these particles until the kinetic freeze-out, $T_{\rm kin}$, where all interactions cease and all unstable resonances have decayed. In such a hybrid model the difference in v_2 due to different hadronic interaction cross sections can be calculated. The VISHNU calculations indeed clearly show that the smaller hadronic cross section leads to a larger v_2 below 2 GeV/c for the ϕ-meson compared to the proton v_2. In the same figure the ϕ-meson v_2 is also plotted for hydrodynamic calculations with two decoupling temperatures, $T_{\rm chem}$ and $T_{\rm kin}$ at 165 and 100 MeV, respectively. This comparison shows that the ϕ-meson v_2 indeed does not change significantly anymore in UrQMD, which models the hadronic contribution. Unfortunately, the uncertainties in the ALICE ϕ-meson v_2 are currently still too large at low-$p_{\rm T}$ to constrain the hadronic contribution.

However, not only for the ϕ-meson v_2 there is a difference between a hybrid and full hydrodynamical model calculations. Strange baryons also have a somewhat smaller hadronic cross section, and even though for the Λ this difference is much smaller it does break the mass hierarchy compared to the proton in the same VISHNU calculation. These calculations compared to the ALICE proton and Λ v_2 measurements are shown in the right panel of Fig. 6. The ALICE measurements of Λ v_2 are much more precise than the ϕ-meson v_2 and clearly show that the mass hierarchy is preserved [72], in clear contrast with VISHNU model predictions.

At intermediate $p_{\rm T}$ the v_2 values of baryons (i.e. protons, Λs, Ξs, Ωs and their antiparticles) become very similar. The meson v_2, π and K, are also the same within uncertainties. The meson v_2 are, however, well below the baryons. This behaviour at intermediate $p_{\rm T}$ is thus very different compared to the mass ordering at low-$p_{\rm T}$. The transverse momentum where the baryon and the pion v_2 cross depends on centrality, moving to higher $p_{\rm T}$ for more central collisions. At these intermediate $p_{\rm T}$ it is argued that the baryons and mesons are formed via constituent quark coalescence [76, 77]. If indeed the baryon and mesons are formed in such a simplified coalescence picture the v_2 of the particle would only depend on the number of its constituent quarks [78]. This implies that all baryons have the same v_2 (independent of their mass) and also all mesons have a single value of v_2. The ratio between baryon and mesons v_2 should be 3/2, the ratio of the number of constituent quarks. Figure 5 shows that ϕ-meson breaks this scaling and is at intermediate $p_{\rm T}$ for the more central collisions closer to the baryons while for the more peripheral closer to the mesons.

To test the number of constituent quark scaling for the other particles, v_2/n_q is plotted versus $p_{\rm T}/n_q$ in Fig. 7, where n_q is the number of constituent quarks. The left and right panels show the scaling for 10–20% and 40–50% centrality, respectively. The data shows that number of constituent quark scaling is only approximate for the baryons and mesons.

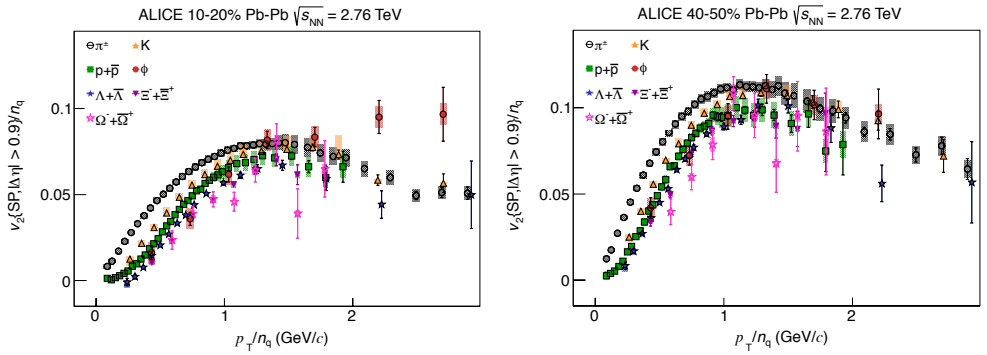

Figure 7. p_{T}-differential elliptic flow of identified particles scaled by the number of constituent quarks for the 10–20% (left) and 40–50% (right) centrality class (figures from [72]).

4.1. Anisotropic flow fluctuations

Due to fluctuations in the initial density profile the initial spatial geometry does not have a smooth almond shape but, instead, a more complex spatial geometry which may possess also odd harmonic symmetry planes. These fluctuations contribute to the measurements of elliptic flow and in addition, are predicted to give rise to odd harmonics like triangular flow v_3.

The difference between $v_n\{2\}$ and $v_n\{4\}$ is sensitive to nonflow and the event-by-event v_n fluctuations. From Eq. 12 and the data in the right panel of Fig. 3, under the assumption that the nonflow contribution $\delta_{2,2}$ is understood and $\sigma_{v_2} \ll \bar{v}_2$, σ_{v_2} can be obtained. The results are plotted in Fig. 8 (left), together with the ratio $\sigma_{v_2}/\bar{v}_2$

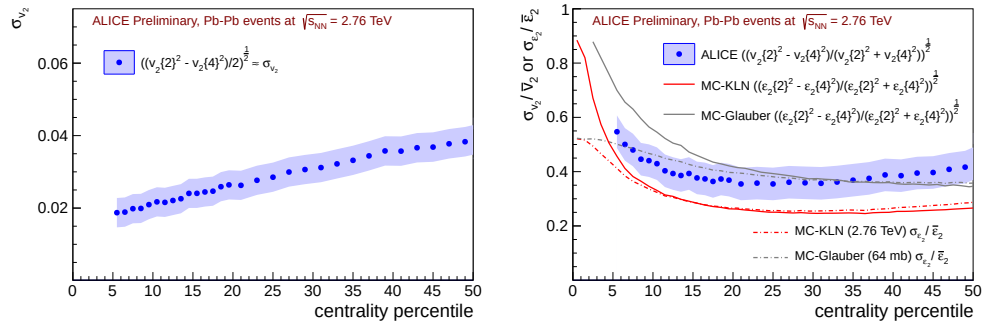
ALICE Preliminary, Pb-Pb events at $\sqrt{s_{NN}}$ = 2.76 TeV
$((v_2\{2\}^2 - v_2\{4\}^2)/2)^{\frac{1}{2}} = \sigma_{v_2}$
σ_{v_2}
centrality percentile
ALICE Preliminary, Pb-Pb events at $\sqrt{s_{NN}}$ = 2.76 TeV
ALICE $((v_2\{2\}^2 - v_2\{4\}^2)/(v_2\{2\}^2 + v_2\{4\}^2))^{\frac{1}{2}}$
MC-KLN $((\varepsilon_2\{2\}^2 - \varepsilon_2\{4\}^2)/(\varepsilon_2\{2\}^2 + \varepsilon_2\{4\}^2))^{\frac{1}{2}}$
MC-Glauber $((\varepsilon_2\{2\}^2 - \varepsilon_2\{4\}^2)/(\varepsilon_2\{2\}^2 + \varepsilon_2\{4\}^2))^{\frac{1}{2}}$
MC-KLN (2.76 TeV) $\sigma_{\varepsilon_2}/\bar{\varepsilon}_2$
MC-Glauber (64 mb) $\sigma_{\varepsilon_2}/\bar{\varepsilon}_2$
$\sigma_{v_2}/\bar{v}_2$ or $\sigma_{\varepsilon_2}/\bar{\varepsilon}_2$
centrality percentile

Figure 8. Left: The magnitude of the event-by-event elliptic flow fluctuations versus collision centrality. Right: Relative event-by-event elliptic flow fluctuations versus collision centrality (figures from [79]).

(right). The ratio $\sigma_{v_2}/\bar{v}_2$ is large $\sim 40\%$, similar to measurements at RHIC [80]. For these large fluctuations $\sigma_{v_2} \ll \bar{v}_2$ is not true, which implies that Eq. 12 is not generally applicable.

The magnitude of the elliptic flow is proportional to ε_2 of the initial density profile, and hydrodynamical model calculations have also shown that the event-by-event fluctuations in the elliptic flow are proportional to that in ε_2. The right panel

of Fig. 8 shows therefore the measured ratio $((v_2\{2\}^2 - v_2\{4\}^2)/(v_2\{2\}^2 + v_2\{4\}^2))^{1/2}$ compared to $((\varepsilon_2\{2\}^2 - \varepsilon_2\{4\}^2)/(\varepsilon_2\{2\}^2 + \varepsilon_2\{4\}^2))^{1/2}$ from a MC-Glauber and MC-KLN model. This comparison does not depend on the assumption that $\sigma_{v_2} \ll \bar{v}_2$ or $\sigma_{\varepsilon_2} \ll \bar{\varepsilon}_2$. The MC-KLN under-predicts the data whereas the MC-Glauber over-predicts the data for more central collisions. To investigate to which extent the ratio plotted in Fig 8 (right) represents $\sigma_{\varepsilon_2}/\bar{\varepsilon}_2$ this ratio is calculated directly from the distributions generated by the two models, that is, without using Eq. 12. For mid-central collisions $\sigma_{\varepsilon_2}/\bar{\varepsilon}_2$ and $((\varepsilon_2\{2\}^2 - \varepsilon_2\{4\}^2)/(\varepsilon_2\{2\}^2 + \varepsilon_2\{4\}^2))^{1/2}$ are very similar in both MC models of the initial state.

Recently it was realised that the odd harmonics are particularly sensitive to both η/s and the initial conditions, which generated strong theoretical and experimental interest [81, 82, 83, 84, 85, 86, 87, 90]. The odd harmonics also give rise to long range correlations in the longitudinal direction. These correlations were first observed at RHIC and initially interpreted as due to jet modifications in the hot and dense matter (i.e. Mach Cones).

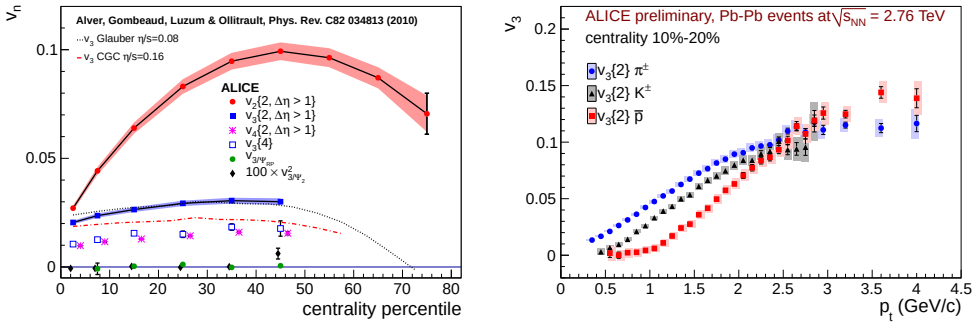

Figure 9. Left: Integrated v_2, v_3 and v_4, full and open squares show $v_3\{2\}$ and $v_3\{4\}$ respectively. In addition we show v^2_{3/Ψ_2} and $v_{3/\Psi_{\rm RP}}$, which represent the triangular flow measured relative to the second order event plane and the reaction plane, respectively. The dashed curves are hydrodynamical predictions [84] (Figure adapted from [87]) Right: The $p_{\rm T}$-differential triangular flow for pions, kaons and antiprotons (Figure taken from [89]).

Figure 9 (left) shows v_2, v_3 and v_4 integrated over $p_{\rm T}$ as a function of centrality. The $v_n\{2\}$ are measured correlating particles which are separated by at least one unit of pseudorapidity, and in addition corrected for the estimated remaining nonflow contribution based on model calculations. The total systematic uncertainty is shown as a band and fully includes this residual correction. The measured v_3 is smaller than v_2 and does not depend strongly on centrality. The hydrodynamic model calculation plotted in the figure show that v_3 is compatible with predictions for Pb-Pb collisions from a calculation with Glauber initial conditions and $\eta/s = 0.08$ and larger than for MC-KLN CGC initial conditions with $\eta/s = 0.16$ [84], suggesting a small value of η/s for the matter produced in these collisions. The $v_3\{4\}$ is about a factor two smaller than the two-particle measurement which can not be understood if the underlying fluctuations are distributed as a 2D Gaussian. Recent studies suggests an elliptic power distribution as an alternative underlying p.d.f., which predicts a non-zero $v_3\{4\}$ and is compatible with the data [91, 92].

For these event-by-event fluctuations of the spatial geometry, the symmetry plane Ψ_3 is expected to be almost uncorrelated with the reaction plane $\Psi_{\rm RP}$ [93], and with

the elliptic flow plane Ψ_2. The correlations between Ψ_3 and $\Psi_{\rm RP}$ is calculated using $v_{3/\Psi_{\rm RP}} = \langle\cos(3\varphi_1 - 3\Psi_{\rm RP})\rangle$ and the correlation between Ψ_3 and Ψ_2 with a five-particle correlator $\langle\cos(3\varphi_1 + 3\varphi_2 - 2\varphi_3 - 2\varphi_4 - 2\varphi_5)\rangle / v_2^3 = v^2_{3/\Psi_2}$. In the left panel of Fig. 9 $v_{3/\Psi_{\rm RP}}$ and v^2_{3/Ψ_2} are shown as a function of centrality. These correlations are indeed, within uncertainties, consistent with zero as expected.

The event-by-event v_n-distributions [94] and the correlations between other planes also have been measured [95] in ATLAS and they are described in detail in another contribution to this volume [96].

In the right panel of Fig. 9, to investigate further the hydrodynamic origin of v_3, the $p_{\rm T}$-differential v_3 of pions, kaons and antiprotons is plotted. It is seen that a similar mass splitting pattern as observed in elliptic flow is also clearly present in triangular flow as well, as is expected if both have the same hydrodynamic origin.

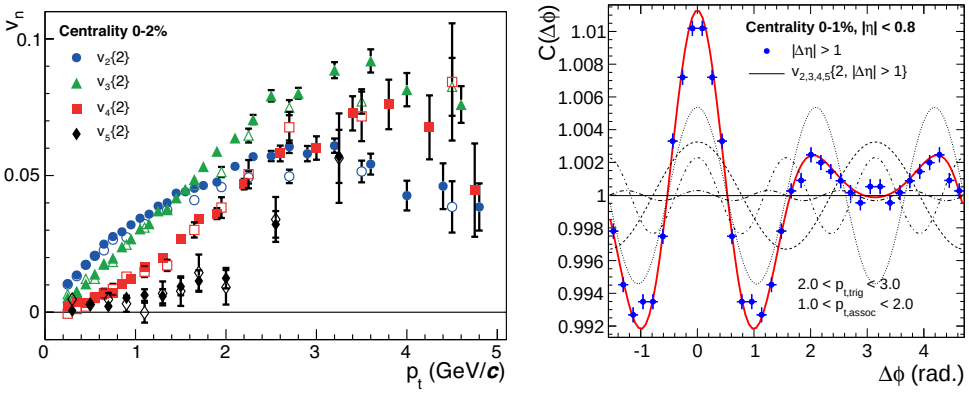

Figure 10. Left: v_2, v_3, v_4, v_5 as a function of transverse momentum. The full, open symbols are for $\Delta\eta > 0.2$ and $\Delta\eta > 1.0$, respectively. Right: The two-particle azimuthal correlation, measured in $0 < \Delta\phi < \pi$ and shown symmetrized over 2π, between a trigger particle with $2 < p_{\rm T} < 3$ GeV/c and an associated particle with $1 < p_{\rm T} < 2$ GeV/c for the 0–1% centrality class. The solid red line shows the sum of the measured anisotropic flow Fourier coefficients v_2, v_3, v_4 and v_5 (dashed lines). Figures taken from [87].

The integrated elliptic flow is dominant compared to the other v_n for all centralities due to the almond shape of the initial spatial density profile. For the most central collisions all the v_n approach each other in magnitude, as is expected when the fluctuations start to dominate all ε_n. For the most 0–2% central collisions the $p_{\rm T}$-differential v_n is plotted in the left panel of Fig. 10. For these very central collisions v_3 becomes equal to v_2 already below 2 GeV/c, while above 3 GeV/c v_3, v_4 and v_5 are all at least equal or larger than v_2 (this behaviour is also confirmed by CMS measurements [88]).

For these very central collisions the large contribution of v_3 is responsible for an interesting structure in the two-particle azimuthal correlation between so called triggered and associated particles. The two-particle azimuthal correlations are measured by calculating:

$$C(\Delta\phi) \equiv \frac{N_{\rm mixed}}{N_{\rm same}} \frac{{\rm d}N_{\rm same}/{\rm d}\Delta\phi}{{\rm d}N_{\rm mixed}/{\rm d}\Delta\phi}, \tag{14}$$

where $\Delta\phi = \phi_{trig} - \phi_{assoc}$, ${\rm d}N_{\rm same}/{\rm d}\Delta\phi$ (${\rm d}N_{\rm mixed}/{\rm d}\Delta\phi$) is the number of associated

particles as function of $\Delta\phi$ within the same (different) event, and $N_{\rm same}$ ($N_{\rm mixed}$) the total number of associated particles in $\mathrm{d}N_{\rm same}/\mathrm{d}\Delta\phi$ ($\mathrm{d}N_{\rm mixed}/\mathrm{d}\Delta\phi$).

Figure 10 (right) shows the azimuthal correlation observed in very central collisions 0–1%, for trigger particles in the range $2 < p_{\rm T} < 3$ GeV/c with associated particles in $1 < p_{\rm T} < 2$ GeV/c for pairs in $|\Delta\eta| > 1$. A clear doubly-peaked correlation structure centered opposite to the trigger particle is observed. This structure also was observed at lower energies in broader centrality bins [97, 98], but only after subtraction of the elliptic flow component. In the past, this two-peak structure was interpreted as an indication for various jet-medium modifications [97, 98] instead of a manifestation of triangular flow [83, 84, 99, 100].

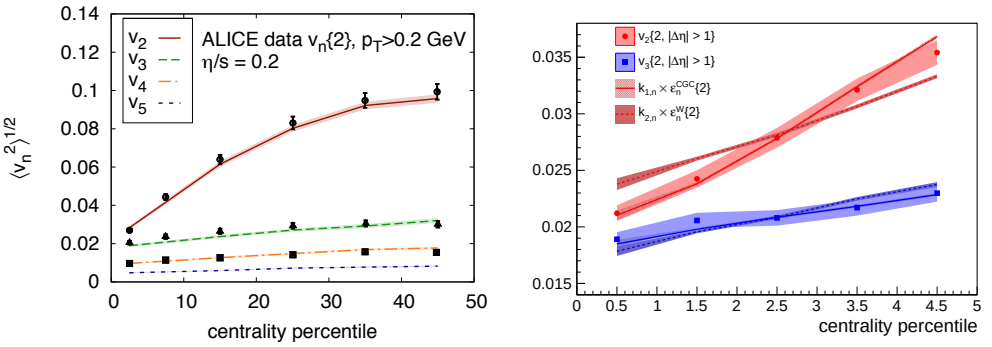

Figure 11. Left: The centrality dependence of $v_n\{2\}$ from 2.76 A TeV Pb+Pb collisions measured by ALICE [87] compared to viscous hydrodynamic model calculations [101] (Figure from [101]). Right: v_2 and v_3 as a function of centrality for the 5% most central collisions compared to calculations of the spatial eccentricities, $\varepsilon_n^W\{2\}$ and $\varepsilon_n^{\rm CGC}\{2\}$. The eccentricities have been scaled to match the 2-3% data using k_1 and k_2 (Figure from [87]).

The hydrodynamical description of the measured v_n is already rather well understood. Figure 11 shows a comparison between the measured v_2, v_3 and v_4 by ALICE [87] and a hydrodynamical model calculation using IP-Glasma initial conditions, together with a kinematic viscosity $\eta/s = 0.2$. These calculations provide a good description of the presently available data for v_n and the $p_{\rm T}$-differential v_n (not shown here).

The v_n depend on both the details of the spatial density distribution and on the kinetic viscosity. Detailed measurements of all the v_n versus centrality provide a way to disentangle both contributions. There is in particular good sensitivity in the most central collisions, because viscous correction do not change much and therefore one is more sensitive to the initial spatial density distributions and its fluctuations. In Fig. 11 (right) $v_2\{2\}$ and $v_3\{2\}$ are plotted in 1% centrality bins for the 5% most central collisions. The $v_3\{2\}$ do not change much versus centrality (as would be expected if v_3 is dominated by event-by-event fluctuations of the initial geometry) while, the $v_2\{2\}$ increase by about 60%. Compared to the centrality dependence of the eccentricities $\varepsilon_n\{2\}$ for initial conditions from MC-KLN CGC and MC-Glauber, it is seen that the weak dependence of $v_3\{2\}$ is described by both models of the initial stage while the relative strong dependence of $v_2\{2\}$ on centrality is only described for the MC-KLN CGC initial conditions.

4.2. Event-shape engineering

Controlling the initial conditions in heavy-ion collisions is of the utmost importance to learn about the properties of high density hot QCD matter. To experimentally control part of the overlap geometry we currently categorise the collisions by their collision centrality or use different collision systems. However with better understanding of the role of the fluctuations in the initial energy density distribution a new tool has become available to control the initial collision geometry.

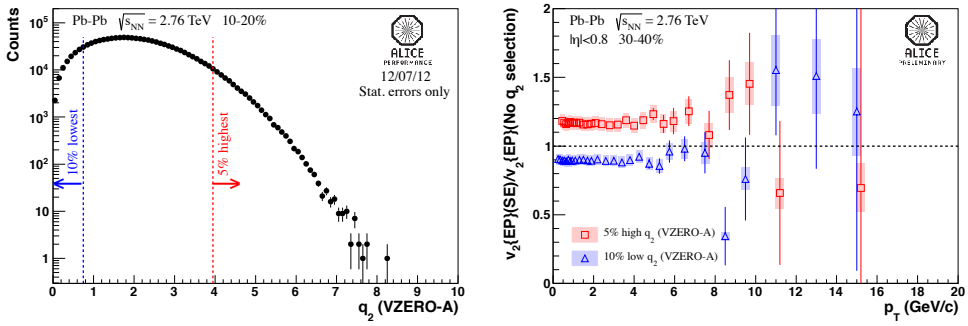

Figure 12. Left: Distribution of q_2 from the VZERO-A ($2.8 \leq \eta \leq 5.1$) for the 10–20% centrality (Figure from [103]). Right: The ratio of unidentified charged particle v_2 between event shape selected and unbiased events (Figure from [103]).

At fixed collision centrality, due to fluctuations in the initial spatial distribution, the v_n differ event-by-event. This can be used to select events with significantly larger or smaller values of v_n compared to the average [102]. In the left panel of Fig. 12 the so-called reduced elliptic flow vector q_2 distribution is plotted. The reduced flow vector is defined as:

$$q_n = Q_n/\sqrt{M}, \tag{15}$$

where Q_n is the flow vector defined in Eq. 6 and M is the multiplicity of the particles used for the flow vector. The nonflow contributions to the measurements are suppressed by choosing the reduced flow vector with a large (pseudo) rapidity separation with respect to where the anisotropic flow or other observables are measured. From the distribution of the reduced elliptic flow vector we can now select the events with the 5% highest and 10% lowest q_2 which have a different event shape. This event-shape engineering of the data sample offers new possibilities to test the properties of the hot and dense QCD matter [102, 103].

The right-panel of Fig. 12 shows the charged particle p_{T}-differential v_2 ratio of event shape selected and unbiased events. As expected for the events with the highest and lowest q_2 the measured $v_2(p_{\mathrm{T}})$ is also higher and lower, respectively. That the ratio of $v_2(p_{\mathrm{T}})$ is flat indicates that the flow fluctuations have a common origin at least up to 6 GeV/c.

In addition to measurements of v_n, this event-shape engineering can be used to understand better many other observables. Examples are azimuthally sensitive femtoscopy and also observables such as final state p_{T} fluctuations, which both clearly would profit from selecting events with extreme values of the anisotropy. However also for observables where v_n is one of the main background contributions, event-shape engineering is an important tool and an example of this is the proposed chiral

magnetic effect. Because the chiral magnetic effect should hardly depend on the fluctuations in the initial spatial density distribution the background v_n contribution could be estimated from measurements in events with the same collision centrality but different event-shape selections. First applications of this new technique for various observables were recently presented [103, 104, 105, 106].

4.3. Anisotropic flow in proton-nucleus collisions?

Azimuthal correlations in proton-proton and proton-nucleus collisions are dominated by near- and away-side jet peaks. In nucleus-nucleus collisions additional correlations due to anisotropic flow are clearly visible. These anisotropic flow correlations quickly become dominant when we look at correlations between particles with a large separation in pseudo-rapidity. However the observation of similar but smaller long range $\Delta\eta$ azimuthal correlations for very high multiplicity proton-proton collision came as a surprise [107]. Because these very high multiplicity events are extremely rare it is currently not clear if this long range $\Delta\eta$ structure, so called ridge, seen in proton-proton and nucleus-nucleus collisions has a common origin.

Data from a dedicated proton-nucleus (p-Pb) run enabled the LHC experiments to collect enough data to investigate if such a ridge also is visible in p-Pb and after that, to investigate in more detail what the origins of these correlations are.

In heavy-ion collisions, events are categorized according to their centrality based on the number of produced particles. In p-Pb the events are also subdivided into different event classes according to the number of produced particles, however for these collisions it is not clear how well this selection corresponds to the centrality of the collision. In ALICE the event classes are defined based on the multiplicity measured at forward pseudo-rapidity and denoted 60–100%, 40–60%, 20–40% and 0–20% from the lowest to the highest multiplicity.

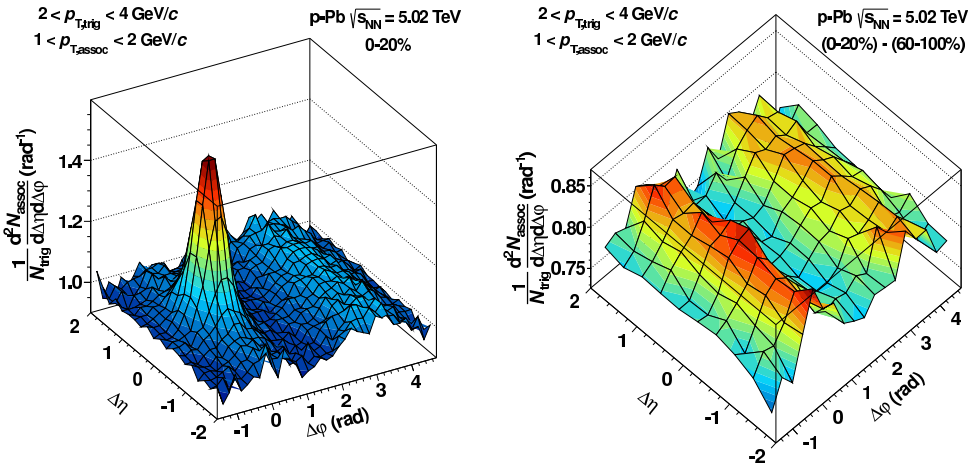

Figure 13. The associated yield per trigger particle in $\Delta\phi$ and $|\Delta\eta|$ for pairs of charged particles in p-Pb collisions. Left the associated yield for the 0–20% multiplicity class and right after the subtraction of the associated yield in the 60–100% multiplicity class (figures taken from [108]). .

In Fig. 13 (left) the $\Delta\varphi$ $\Delta\eta$ correlations measured by ALICE in p-Pb collisions

at $\sqrt{s_{NN}} = 5.02$ TeV are plotted [108] for the events in the multiplicity class 0–20%. A clear ridge structure at $\Delta\varphi = \pi$ (the away side ridge) is observed, as was also already seen in very high multiplicity p-p collisions by CMS [107]. At $\Delta\varphi = 0$ a clear jet-like peak is observed, which is, however, not isolated but situated on top of a ridge as well (the so-called near-side ridge). This near-side ridge is clearly visible in high multiplicity p-Pb collisions [108, 109, 110]. To quantify the change from low to high-multiplicity events, the correlated per trigger yield of the lowest multiplicity class is subtracted from the highest multiplicity class. The remaining distribution is shown in Fig. 13 (right), and exhibits a clear double ridge structure. These two ridges, one on the near-side and one on the away-side, are very similar [108, 111].

Theoretically the origin of the observed ridge structure in p-Pb collisions is still the subject of speculation [112, 113, 114, 115]. Currently, three theoretical proposals exist which might explain (part of) the observed azimuthal correlations. The first proposal is that the energy density achieved in p-Pb collisions is high enough that hydrodynamics using a Lattice QCD EoS can be used to describe the underlying physics. In that case, the spatial anisotropies in the initial state of a p-Pb collisions would generate anisotropic flow, resulting in significant values of v_2 and v_3 [112]. The second proposal is inspired by the Color Glass Condensate description and claims that the ridge originates from collimated, in relative azimuthal angle, two-gluon production [113]. The third explanation is a combination of the previous two which invokes an CGC initial state with a finite number of sources which define the initial spatial anisotropy [114].

While these theoretical models can explain many of the observations and, in fact, even predicted these double ridge structures [112], it is currently not clear if one can do an apples to apples comparison between theory calculations and experimental data. Most of the comparisons rely on the fact that we either compare events with similar collision centrality (and some assumed relation with the initial spatial distribution) or compare events with a similar number of sources of particle production. In p-Pb, the correlation between the collision geometry or the number of sources to the measured multiplicity, which is used to bin the experimental data, is under investigation and currently not well established. Therefore, in the remainder of the section, we focus only on the question if in experimental data the ridge observed in two-particle correlations is consistent with expectations of anisotropic flow. If this is the case, it should result in a well defined behaviour of the multi-particle cumulants and a clear mass hierarchy in the p_{T}-differential v_2 in p-Pb.

The two-particle cumulant is plotted as a function of the charged particle multiplicity in p-Pb in the left panel of Fig. 14 for four different gaps in pseudo-rapidity. When there is no gap in pseudo-rapidity between the particles the jet contribution clearly dominates and the two-particle cumulant decreases strongly with increasing multiplicity. This is expected due to simple combinatorics. With increasing gap in pseudo-rapidity the multiplicity dependence clearly changes. For the two-particle cumulant with $|\Delta\eta| > 1.4$ an increase with multiplicity is observed, which is compatible with the suppression of the jet-like peak in Fig. 13 (left) and the observed increase of the double ridge with increasing event multiplicity.

To investigate if this two-particle correlation results from a multi-particle correlation we plot in Fig. 14 (middle) the four-particle cumulant as function of multiplicity. For the four-particle cumulant no gap in pseudo-rapidity is applied. For the events with a lower multiplicity the four-particle cumulant is positive which is incompatible with a dominant contribution coming from anisotropic flow. For events

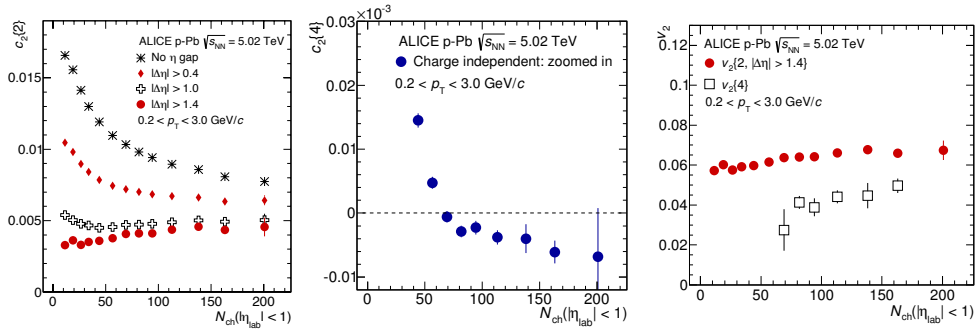

Figure 14. Two and multi-particle azimuthal correlations as function of the charged particle multiplicity in p-Pb collisions measured by ALICE. Left: The two-particle cumulant $c_2\{2\}$ for four different gaps in pseudo-rapidity. Middle: The four-particle cumulant $c_2\{4\}$. Right: The corresponding $v_2\{2\}$ and $v_2\{4\}$ (figures taken from [116]).

with a multiplicity of about 70 and higher the four-particle cumulant becomes negative, which is a prerequisite to determine the corresponding $v_2\{4\}$.

In the right panel of Fig. 14 the $v_2\{2\}$ and $v_2\{4\}$ are plotted versus multiplicity. The $v_2\{2\}$ is larger than $v_2\{4\}$ for the whole multiplicity range, similar to what is observed in Pb-Pb collisions [116, 117, 110]. The difference between $v_2\{2\}$ and $v_2\{4\}$ is indicative of anisotropic flow fluctuations but has also clearly a significant nonflow contribution. Measurements of $v_2\{6\}$ and $v_2\{8\}$ also have been performed in p-Pb collisions at the LHC by CMS [106] (not shown here) and are found to be compatible with $v_2\{4\}$. In addition also a significant value of v_3 was observed. Within current uncertainties all this is consistent with a elliptic power probability distribution [92] of a limited number of sources in the initial spatial distribution ε [91, 92].

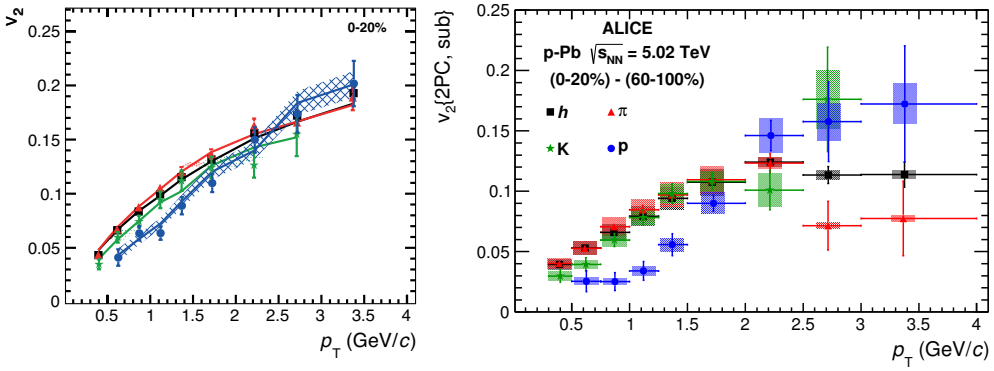

Figure 15. Left: p_T-differential v_2 for all charged particles, pions, kaons and protons in p-Pb collisions for the 0–20% multiplicity class. The solid lines are the v_2 obtained from particles correlated at fixed p_T with particles from the full p_T range. The symbols are the v_2 obtained from correlating particles in the same p_T interval. Right: The p_T-differential v_2 for the 0–20% multiplicity class after subtracting the per-trigger yield of the 60–100% multiplicity class. (figures taken from [118]).

The p_T-differential v_2 for different particles exhibits a characteristic mass

hierarchy in Pb-Pb collisions, which in hydrodynamics is understood due to a mass dependent blueshift which is stronger in the flow plane. If the ridge structures observed in p-Pb collisions also originate from a hydrodynamic expansion we would expect to also observe a mass hierarchy in $v_2(p_{\mathrm{T}}, m)$ for these collisions. In Fig. 15 the p_{T}-differential v_2 is plotted for the 0–20% multiplicity class. The left panel shows the results for the charged particles as well as for the pions, kaons and protons separately. The results were obtained using a pseudo-rapidity gap of $|\Delta\eta| = 0.8$. The v_2 are calculated correlating the particles from a certain p_{T} interval with particles from the full p_{T} range (solid lines), and compared to another procedure were both particles are taken from the same p_{T} interval (symbols). These results should agree if the measurement is dominated by correlations of each of the particles with a common flow plane and the v_n fluctuations are p_{T} independent. We observe that for the 0–20% multiplicity class the lines and symbols are in agreement and that a clear mass hierarchy is observed [118].

To again quantify the change from low to high-multiplicity events, the right panel of Fig. 15 shows the resulting $v_2(p_{\mathrm{T}}, m)$ after subtracting the per-trigger yield of the 60–100% multiplicity class from that in the 0–20% multiplicity class. After this subtraction the mass hierarchy becomes even more pronounced.

The correlation measurements in p-Pb show clear evidence for multi-particle correlations and are in qualitative agreement with hydrodynamical expectations. However, currently it is far from clear what the underlying microscopic mechanism is which is responsible for this behaviour.

5. SUMMARY AND OUTLOOK

Anisotropic flow studies at the LHC have already produced a wealth of new results and many of the measurements in Pb-Pb collision at LHC energies are relatively well understood in terms of a strongly coupled quark-gluon liquid as modelled in state of the art hydrodynamic model calculations. The initial density profile and its event-by-event fluctuations, which are currently the largest uncertainties in these calculations, are in particular much better understood due to the detailed v_n measurements. At the same time there are also still many open questions which need to be addressed to reach the goal of a quantitative reliable description of heavy-ion collisions:

- The topic which currently gets considerable theoretical attention is the contribution to the flow from the very early stage (initial velocity profiles) [119, 120, 121, 122, 123, 124].
- In addition to the contribution to the flow from the very early stage there are also still open questions about the contribution from the late hadronic stage [17] and due to the particle production mechanism [78].
- Another hotly debated topic is if some of the angular correlations observed in p-p and p-Pb collisions, which traditionally are used as a reference for nucleus-nucleus collisions, are also related to the initial geometry.
- A topic discussed in other contributions to this volume is the flow of rare probes. It is important to see how the heavy quarks participate in the flow [125, 126, 127, 128, 129, 130, 131, 132] but perhaps even more interesting is understanding the large flow observed for direct photons [133, 134, 135, 136, 137].

While most of the measured v_n were discussed in this review, the first harmonic v_1 was notably missing. The v_1 is sensitive to different interesting physics

contributions [138, 139, 99, 140, 141, 142, 143, 144] that, unfortunately, are difficult to disentangle. In this volume one review article focusses mainly on this harmonic [145].

Finally, because flow is closely related to the geometry of the collision, a by-product of the flow analysis methods is the access to important orientation axes in a collision, like the orientation of the reaction-plane spanned by the beam axis and the impact parameter that connects the centre of the colliding nuclei. Exploration of the sensitivity of observables to the reaction- or flow-planes opens the road to very interesting physics analyses like the detailed investigation of jet energy loss [68, 69, 146] and the possible effects of the large magnetic fields generated by the colliding nuclei [147, 148, 149, 150, 151, 152].

Acknowledgements: I would like to thank Ante Bilandzic, Alexandru Florin Dobrin and You Zhou for the useful comments. The work of RS was partially supported by the Stichting voor Fundamenteel Onderzoek der Materie (FOM), Nederlandse Organisatie voor Wetenschappelijk Onderzoek (NWO), and the Gastprogramm des Bayerischen Wissenschaftministerium.

[1] K. G. Wilson, Phys. Rev. D **10**, 2445 (1974).
[2] E. V. Shuryak, Phys. Lett. B **78**, 150 (1978) [Sov. J. Nucl. Phys. **28**, 408 (1978)] [Yad. Fiz. **28**, 796 (1978)] Phys. Rept. **61**, 71 (1980).
[3] G. F. Chapline, M. H. Johnson, E. Teller, and M. S. Weiss. Phys. Rev. D8:4302–4308, 1973.
[4] T. D. Lee and G. C. Wick. Phys. Rev. D9:2291, 1974.
[5] T. D. Lee. Phys. Rev. D19:1802, 1979.
[6] John C. Collins and M. J. Perry. Phys. Rev. Lett. 34:1353, 1975.
[7] Robert D. Pisarski and Frank Wilczek. Phys. Rev. D29:338–341, 1984.
[8] K. Rajagopal and F. Wilczek, In *Shifman, M. (ed.): At the frontier of particle physics, vol. 3* 2061-2151 [hep-ph/0011333].
[9] J. -Y. Ollitrault, Phys. Rev. D **46**, 229 (1992).
[10] P. Huovinen and P. Petreczky, Nucl. Phys. A **837**, 26 (2010) [arXiv:0912.2541 [hep-ph]].
[11] S. Voloshin and Y. Zhang, Z. Phys. C **70**, 665 (1996) [hep-ph/9407282].
[12] P. Huovinen and P. V. Ruuskanen, Ann. Rev. Nucl. Part. Sci. **56**, 163 (2006) [nucl-th/0605008].
[13] S. A. Voloshin, A. M. Poskanzer and R. Snellings, arXiv:0809.2949 [nucl-ex].
[14] D. A. Teaney, arXiv:0905.2433 [nucl-th].
[15] U. Heinz and R. Snellings, Ann. Rev. Nucl. Part. Sci. **63**, 123 (2013) [arXiv:1301.2826 [nucl-th]].
[16] C. Gale, S. Jeon and B. Schenke, Int. J. Mod. Phys. A **28**, 1340011 (2013) [arXiv:1301.5893 [nucl-th]].
[17] M. Luzum and H. Petersen, J. Phys. G **41**, 063102 (2014) [arXiv:1312.5503 [nucl-th]].
[18] D. J. Gross and F. Wilczek, Phys. Rev. Lett. **30**, 1343 (1973).
[19] H. D. Politzer, Phys. Rev. Lett. **30**, 1346 (1973).
[20] S. Nadkarni, Phys. Rev. D **33**, 3738 (1986).
[21] K. H. Ackermann *et al.* [STAR Collaboration], Phys. Rev. Lett. **86**, 402 (2001) [nucl-ex/0009011].
[22] S. S. Adler *et al.* [PHENIX Collaboration], Phys. Rev. Lett. **91**, 182301 (2003) [nucl-ex/0305013].
[23] K. Aamodt *et al.* [ALICE Collaboration], Phys. Rev. Lett. **105**, 252302 (2010) [arXiv:1011.3914 [nucl-ex]].
[24] G. Aad *et al.* [ATLAS Collaboration], Phys. Lett. B **707**, 330 (2012) [arXiv:1108.6018 [hep-ex]].
[25] S. Chatrchyan *et al.* [CMS Collaboration], Phys. Rev. C **87**, 014902 (2013) [arXiv:1204.1409 [nucl-ex]].
[26] D. Teaney, Phys. Rev. C **68**, 034913 (2003) [nucl-th/0301099].
[27] P. Romatschke and U. Romatschke, Phys. Rev. Lett. **99**, 172301 (2007) [arXiv:0706.1522 [nucl-th]].
[28] M. Luzum and P. Romatschke, Phys. Rev. C **78**, 034915 (2008) [Erratum-ibid. C **79**, 039903 (2009)] [arXiv:0804.4015 [nucl-th]].
[29] J. M. Maldacena, Adv. Theor. Math. Phys. **2** (1998) 231 [hep-th/9711200].
[30] P. Kovtun, D. T. Son and A. O. Starinets, Phys. Rev. Lett. **94**, 111601 (2005) [hep-th/0405231].
[31] L. P. Csernai, J. .I. Kapusta and L. D. McLerran, Phys. Rev. Lett. **97**, 152303 (2006) [nucl-th/0604032].

[32] R. A. Lacey, N. N. Ajitanand, J. M. Alexander, P. Chung, W. G. Holzmann, M. Issah, A. Taranenko and P. Danielewicz *et al.*, Phys. Rev. Lett. **98**, 092301 (2007) [nucl-ex/0609025].
[33] M. Miller and R. Snellings, nucl-ex/0312008.
[34] R. Andrade, F. Grassi, Y. Hama, T. Kodama and O. Socolowski, Jr., Phys. Rev. Lett. **97**, 202302 (2006) [nucl-th/0608067].
[35] B. Alver *et al.* [PHOBOS Collaboration], Phys. Rev. Lett. **98**, 242302 (2007) [nucl-ex/0610037].
[36] H. Petersen, J. Steinheimer, G. Burau, M. Bleicher and H. Stocker, Phys. Rev. C **78**, 044901 (2008) [arXiv:0806.1695 [nucl-th]].
[37] C. Flensburg, arXiv:1108.4862 [nucl-th].
[38] N. Borghini, P. M. Dinh and J. -Y. Ollitrault, Phys. Rev. C **64**, 054901 (2001) [nucl-th/0105040].
[39] A. Bilandzic, R. Snellings and S. Voloshin, Phys. Rev. C **83**, 044913 (2011) [arXiv:1010.0233 [nucl-ex]].
[40] A. Bilandzic, C. H. Christensen, K. Gulbrandsen, A. Hansen and Y. Zhou, Phys. Rev. C **89**, 064904 (2014) [arXiv:1312.3572 [nucl-ex]].
[41] P. Danielewicz and G. Odyniec, Phys. Lett. B **157**, 146 (1985).
[42] Kovner A, McLerran LD, Weigert H. *Phys. Rev. D* 52:6231 (1995)
[43] Kovchegov YV, Rischke DH. *Phys. Rev. C* 56:1084 (1997)
[44] Krasnitz A, Venugopalan R. *Nucl. Phys. B* 557:237 (1999); *Phys. Rev. Lett.* 84:4309 (2000); *ibid.* 86:1717 (2001)
[45] Lappi T. *Phys. Rev. C* 67:054903 (2003); Lappi T, McLerran LD. *Nucl. Phys. A* 772:200 (2006)
[46] Schenke B, Tribedy P, Venugopalan R. *Phys. Rev. Lett.* 108:252301 (2012); *Phys. Rev. C* 86:034908 (2012)
[47] Müller B, Schäfer A. *Phys. Rev. D* 85:114030 (2012)
[48] Dumitru A, Nara Y. *Phys. Rev. C* 85:034907 (2012)
[49] Miller ML, Reygers K, Sanders SJ, Steinberg P. Ann. Rev. Nucl. Part. Sci. 57:205 (2007)
[50] Drescher HJ, Nara Y. *Phys. Rev. C* 75:034905 (2007); *ibid.* 76:041903(R) (2007)
[51] Bartels J, Golec-Biernat KJ, Kowalski H. *Phys. Rev. D* 66:014001 (2002); Kowalski H, Teaney D. *Phys. Rev. D* 68:114005 (2003)
[52] Moreland JS, Qiu Z, Heinz U. arXiv:1210.5508 [nucl-th] (2012)
[53] Kovchegov YV, Levin E. *Quantum Chromodynamics at High Energy*. Cambridge University Press (2012)
[54] F. G. Gardim, F. Grassi, M. Luzum and J. -Y. Ollitrault, Phys. Rev. C **85**, 024908 (2012) [arXiv:1111.6538 [nucl-th]].
[55] Teaney D, Yan L. *Phys. Rev. C* 86:044908 (2012); arXiv:1210.5026 [nucl-th] (2012)
[56] Qiu Z, Heinz U. *Phys. Lett. B* 717:261 (2012)
[57] Baier R, Romatschke P, Son DT, Starinets AO, Stephanov MA. *JHEP* 0804:100 (2008)
[58] Muronga A. *Phys. Rev. C* 69:034903 (2004)
[59] Heinz U, Song H, Chaudhuri AK. *Phys. Rev. C* 73:034904 (2006)
[60] Song H, Heinz U. *Phys. Lett. B* 658:279 (2008); *Phys. Rev. C* 77:064901 (2008)
[61] Song H, Heinz U. *Phys. Rev. C* 78:024902 (2008)
[62] Molnar E, Niemi H, Rischke DH. *Eur. Phys. J. C* **65**, 615 (2010)
[63] Denicol GS, Koide T, Rischke DH. *Phys. Rev. Lett.* 105:162501 (2010)
[64] Denicol GS, Niemi H, Molnar E, Rischke DH. *Phys. Rev. D* **85**, 114047 (2012); Denicol GS, Molnar E, Niemi H, Rischke DH. arXiv:1206.1554 [nucl-th] (2012); Denicol GS, Niemi H, Bouras I, Molnar E, Xu Z, Rischke DH, Greiner C. arXiv:1207.6811 [nucl-th] (2012)
[65] El A, Xu Z, Greiner C. *Phys. Rev. C* 81:041901(R) (2010)
[66] S. S. Gubser, I. R. Klebanov and A. W. Peet, Phys. Rev. D **54**, 3915 (1996) [hep-th/9602135].
[67] A. Bilandzic [ALICE Collaboration], J. Phys. G **38**, 124052 (2011) [arXiv:1106.6209 [nucl-ex]].
[68] B. Abelev *et al.* [ALICE Collaboration], Phys. Lett. B **719**, 18 (2013) [arXiv:1205.5761 [nucl-ex]].
[69] R. J. M. Snellings, A. M. Poskanzer and S. A. Voloshin, nucl-ex/9904003.
[70] W. A. Horowitz and M. Gyulassy, J. Phys. G **38**, 124114 (2011) [arXiv:1107.2136 [hep-ph]].
[71] B. Abelev *et al.* [ALICE Collaboration], Phys. Rev. C **88**, no. 4, 044910 (2013) [arXiv:1303.0737 [hep-ex]].
[72] B. B. Abelev *et al.* [ALICE Collaboration], arXiv:1405.4632 [nucl-ex].
[73] P. Huovinen, P. F. Kolb, U. W. Heinz, P. V. Ruuskanen and S. A. Voloshin, Phys. Lett. B **503**, 58 (2001) [hep-ph/0101136].
[74] C. Adler *et al.* [STAR Collaboration], Phys. Rev. Lett. **87**, 182301 (2001) [nucl-ex/0107003].
[75] H. Song, S. Bass and U. W. Heinz, Phys. Rev. C **89**, 034919 (2014) [arXiv:1311.0157 [nucl-th]].
[76] V. Greco, C. M. Ko and P. Levai, Phys. Rev. Lett. **90**, 202302 (2003) [nucl-th/0301093].

[77] V. Greco, C. M. Ko and P. Levai, Phys. Rev. C **68**, 034904 (2003) [nucl-th/0305024].
[78] D. Molnar and S. A. Voloshin, Phys. Rev. Lett. **91**, 092301 (2003) [nucl-th/0302014].
[79] R. Snellings, J. Phys. G **38**, 124013 (2011) [arXiv:1106.6284 [nucl-ex]].
[80] B. Alver *et al.* [PHOBOS Collaboration], Phys. Rev. Lett. **104**, 142301 (2010)
[81] J. Takahashi, B. M. Tavares, W. L. Qian, R. Andrade, F. Grassi, Y. Hama, T. Kodama and N. Xu, Phys. Rev. Lett. **103**, 242301 (2009) [arXiv:0902.4870 [nucl-th]].
[82] P. Sorensen, J. Phys. G **37**, 094011 (2010) [arXiv:1002.4878 [nucl-ex]].
[83] B. Alver and G. Roland, Phys. Rev. C **81**, 054905 (2010) [Erratum-ibid. C **82**, 039903 (2010)] [arXiv:1003.0194 [nucl-th]].
[84] B. H. Alver, C. Gombeaud, M. Luzum and J. -Y. Ollitrault, Phys. Rev. C **82**, 034913 (2010) [arXiv:1007.5469 [nucl-th]].
[85] S. Floerchinger and U. A. Wiedemann, Phys. Rev. C **88**, 044906 (2013) [arXiv:1307.7611 [hep-ph]].
[86] S. Floerchinger and U. A. Wiedemann, arXiv:1405.4393 [hep-ph].
[87] K. Aamodt *et al.* [ALICE Collaboration], Phys. Rev. Lett. **107**, 032301 (2011) [arXiv:1105.3865 [nucl-ex]].
[88] S. Chatrchyan *et al.* [CMS Collaboration], JHEP **1402**, 088 (2014) [arXiv:1312.1845 [nucl-ex]].
[89] M. Krzewicki [ALICE Collaboration], J. Phys. G **38**, 124047 (2011) [arXiv:1107.0080 [nucl-ex]].
[90] A. Adare *et al.* [PHENIX Collaboration], Phys. Rev. Lett. **107**, 252301 (2011) [arXiv:1105.3928 [nucl-ex]].
[91] L. Yan and J. -Y. Ollitrault, Phys. Rev. Lett. **112**, 082301 (2014) [arXiv:1312.6555 [nucl-th]].
[92] L. Yan, J. -Y. Ollitrault and A. M. Poskanzer, arXiv:1405.6595 [nucl-th].
[93] A. M. Poskanzer and S. A. Voloshin, Phys. Rev. C **58**, 1671 (1998) [nucl-ex/9805001].
[94] G. Aad *et al.* [ATLAS Collaboration], JHEP **1311**, 183 (2013) [arXiv:1305.2942 [hep-ex]].
[95] G. Aad *et al.* [ATLAS Collaboration], arXiv:1403.0489 [hep-ex].
[96] J. Jia, This Volume, arXiv:1407.6057 [nucl-ex].
[97] A. Adare *et al.* [PHENIX Collaboration], Phys. Rev. C **78**, 014901 (2008) [arXiv:0801.4545 [nucl-ex]].
[98] M. M. Aggarwal *et al.* [STAR Collaboration], Phys. Rev. C **82**, 024912 (2010) [arXiv:1004.2377 [nucl-ex]].
[99] D. Teaney and L. Yan, Phys. Rev. C **83**, 064904 (2011) [arXiv:1010.1876 [nucl-th]].
[100] M. Luzum, Phys. Lett. B **696**, 499 (2011) [arXiv:1011.5773 [nucl-th]].
[101] C. Gale, S. Jeon, B. Schenke, P. Tribedy and R. Venugopalan, Phys. Rev. Lett. **110**, 012302 (2013) [arXiv:1209.6330 [nucl-th]].
[102] J. Schukraft, A. Timmins and S. A. Voloshin, Phys. Lett. B **719**, 394 (2013) [arXiv:1208.4563 [nucl-ex]].
[103] A. Dobrin [ALICE Collaboration], Nucl. Phys. A **904-905**, 455c (2013) [arXiv:1211.5348 [nucl-ex]].
[104] R. A. Lacey, D. Reynolds, A. Taranenko, N. N. Ajitanand, J. M. Alexander, F. -H. Liu, Y. Gu and A. Mwai, arXiv:1311.1728 [nucl-ex].
[105] P. Huo, J. Jia and S. Mohapatra, arXiv:1311.7091 [nucl-ex].
[106] S. Mohapatra for the ATLAS Collaboration, proceedings for QM 2014; ATLAS-CONF-2014-022, http://cds.cern.ch/record/1702980 and other presentations at QM2014, Darmstad.
[107] V. Khachatryan *et al.* [CMS Collaboration], JHEP **1009**, 091 (2010) [arXiv:1009.4122 [hep-ex]].
[108] B. Abelev *et al.* [ALICE Collaboration], Phys. Lett. B **719**, 29 (2013) [arXiv:1212.2001 [nucl-ex]].
[109] S. Chatrchyan *et al.* [CMS Collaboration], Phys. Lett. B **718**, 795 (2013) [arXiv:1210.5482 [nucl-ex]].
[110] S. Chatrchyan *et al.* [CMS Collaboration], Phys. Lett. B **724**, 213 (2013) [arXiv:1305.0609 [nucl-ex]].
[111] G. Aad *et al.* [ATLAS Collaboration], Phys. Rev. Lett. **110**, 182302 (2013) [arXiv:1212.5198 [hep-ex]].
[112] P. Bozek and W. Broniowski, Phys. Lett. B **718**, 1557 (2013) [arXiv:1211.0845 [nucl-th]].
[113] K. Dusling and R. Venugopalan, Phys. Rev. D **87**, no. 5, 054014 (2013) [arXiv:1211.3701 [hep-ph]].
[114] A. Dumitru, T. Lappi and L. McLerran, Nucl. Phys. A **922**, 140 (2014) [arXiv:1310.7136 [hep-ph]].
[115] G. Basar and D. Teaney, arXiv:1312.6770 [nucl-th].
[116] B. B. Abelev *et al.* [ALICE Collaboration], arXiv:1406.2474 [nucl-ex].
[117] G. Aad *et al.* [ATLAS Collaboration], Phys. Lett. B **725**, 60 (2013) [arXiv:1303.2084 [hep-ex]].
[118] B. B. Abelev *et al.* [ALICE Collaboration], Phys. Lett. B **726**, 164 (2013) [arXiv:1307.3237

[nucl-ex]].
[119] F. Becattini, F. Piccinini and J. Rizzo, Phys. Rev. C **77**, 024906 (2008) [arXiv:0711.1253 [nucl-th]].
[120] J. Vredevoogd and S. Pratt, Phys. Rev. C **79**, 044915 (2009) [arXiv:0810.4325 [nucl-th]].
[121] M. P. Heller, D. Mateos, W. van der Schee and D. Trancanelli, Phys. Rev. Lett. **108**, 191601 (2012) [arXiv:1202.0981 [hep-th]].
[122] J. Casalderrey-Solana, M. P. Heller, D. Mateos and W. van der Schee, Phys. Rev. Lett. **111**, 181601 (2013) [arXiv:1305.4919 [hep-th]].
[123] W. van der Schee, P. Romatschke and S. Pratt, Phys. Rev. Lett. **111**, no. 22, 222302 (2013) [arXiv:1307.2539].
[124] R. J. Fries and G. Chen, arXiv:1407.1903 [nucl-th].
[125] E. Abbas *et al.* [ALICE Collaboration], Phys. Rev. Lett. **111**, 162301 (2013) [arXiv:1303.5880 [nucl-ex]].
[126] B. Abelev *et al.* [ALICE Collaboration], Phys. Rev. Lett. **111**, 102301 (2013) [arXiv:1305.2707 [nucl-ex]].
[127] B. B. Abelev *et al.* [ALICE Collaboration], arXiv:1405.2001 [nucl-ex].
[128] J. Uphoff, O. Fochler, Z. Xu and C. Greiner, Phys. Rev. C **84**, 024908 (2011) [arXiv:1104.2295 [hep-ph]].
[129] O. Fochler, J. Uphoff, Z. Xu and C. Greiner, J. Phys. G **38**, 124152 (2011) [arXiv:1107.0130 [hep-ph]].
[130] S. Batsouli, S. Kelly, M. Gyulassy and J. L. Nagle, Phys. Lett. B **557**, 26 (2003) [nucl-th/0212068].
[131] V. Greco, C. M. Ko and R. Rapp, Phys. Lett. B **595**, 202 (2004) [nucl-th/0312100].
[132] Y. Liu, N. Xu and P. Zhuang, Nucl. Phys. A **834**, 317C (2010) [arXiv:0910.0959 [nucl-th]].
[133] A. Adare *et al.* [PHENIX Collaboration], Phys. Rev. Lett. **109**, 122302 (2012) [arXiv:1105.4126 [nucl-ex]].
[134] D. Lohner [ALICE Collaboration], J. Phys. Conf. Ser. **446**, 012028 (2013) [arXiv:1212.3995 [hep-ex]].
[135] R. Chatterjee, E. S. Frodermann, U. W. Heinz and D. K. Srivastava, Phys. Rev. Lett. **96**, 202302 (2006) [nucl-th/0511079].
[136] C. Shen, U. WHeinz, J. -F. Paquet, I. Kozlov and C. Gale, arXiv:1308.2111 [nucl-th].
[137] C. Shen, U. Heinz, J. -F. Paquet and C. Gale, arXiv:1403.7558 [nucl-th].
[138] G. Aad *et al.* [ATLAS Collaboration], Phys. Rev. C **86**, 014907 (2012) [arXiv:1203.3087 [hep-ex]].
[139] B. Abelev *et al.* [ALICE Collaboration], Phys. Rev. Lett. **111**, no. 23, 232302 (2013) [arXiv:1306.4145 [nucl-ex]].
[140] M. Luzum and J. -Y. Ollitrault, Phys. Rev. Lett. **106**, 102301 (2011) [arXiv:1011.6361 [nucl-ex]].
[141] F. G. Gardim, F. Grassi, Y. Hama, M. Luzum and J. -Y. Ollitrault, Phys. Rev. C **83**, 064901 (2011) [arXiv:1103.4605 [nucl-th]].
[142] E. Retinskaya, M. Luzum and J. -Y. Ollitrault, Phys. Rev. Lett. **108**, 252302 (2012) [arXiv:1203.0931 [nucl-th]].
[143] R. J. M. Snellings, H. Sorge, S. A. Voloshin, F. Q. Wang and N. Xu, Phys. Rev. Lett. **84**, 2803 (2000) [nucl-ex/9908001].
[144] L. P. Csernai and D. Rohrich, Phys. Lett. B **458**, 454 (1999) [nucl-th/9908034].
[145] L. P. Csernai and H. Stoecker, arXiv:1406.1153 [nucl-th].
[146] S. A. Bass, C. Gale, A. Majumder, C. Nonaka, G. -Y. Qin, T. Renk and J. Ruppert, Phys. Rev. C **79**, 024901 (2009) [arXiv:0808.0908 [nucl-th]].
[147] B. Abelev *et al.* [ALICE Collaboration], Phys. Rev. Lett. **110**, 012301 (2013) [arXiv:1207.0900 [nucl-ex]].
[148] B. I. Abelev *et al.* [STAR Collaboration], Phys. Rev. Lett. **103**, 251601 (2009) [arXiv:0909.1739 [nucl-ex]].
[149] D. E. Kharzeev, L. D. McLerran and H. J. Warringa, Nucl. Phys. A **803**, 227 (2008) [arXiv:0711.0950 [hep-ph]].
[150] K. Fukushima, D. E. Kharzeev and H. J. Warringa, Phys. Rev. D **78**, 074033 (2008) [arXiv:0808.3382 [hep-ph]].
[151] S. A. Voloshin, Phys. Rev. C **70**, 057901 (2004) [hep-ph/0406311].
[152] U. Gursoy, D. Kharzeev and K. Rajagopal, Phys. Rev. C **89**, 054905 (2014) [arXiv:1401.3805 [hep-ph]].